Topics in Applied Physics
Volume 114

Topics in Applied Physics

Topics in Applied Physics is a well-established series of review books, each of which presents a comprehensive survey of a selected topic within the broad area of applied physics. Edited and written by leading research scientists in the field concerned, each volume contains review contributions covering the various aspects of the topic. Together these provide an overview of the state of the art in the respective field, extending from an introduction to the subject right up to the frontiers of contemporary research.
Topics in Applied Physics is addressed to all scientists at universities and in industry who wish to obtain an overview and to keep abreast of advances in applied physics. The series also provides easy but comprehensive access to the fields for newcomers starting research.
Contributions are specially commissioned. The Managing Editors are open to any suggestions for topics coming from the community of applied physicists no matter what the field and encourage prospective editors to approach them with ideas.

Robert W. Boyd, Svetlana G. Lukishova,
Y. R. Shen (Eds.)

Self-focusing: Past and Present

Fundamentals and Prospects

Springer

Robert W. Boyd
University of Rochester
Rochester, NY
boyd@optics.rochester.edu

Svetlana G. Lukishova
University of Rochester
Rochester, NY
sluk@lle.rochester.edu

Y.R. Shen
University of California
Berkeley, CA
shenyr@physics.berkeley.edu

ISSN: 0303-4216
ISBN: 978-0-387-32147-9 e-ISBN: 978-0-387-34727-1
DOI 10.1007/978-0-387-34727-1

Library of Congress Control Number: 2008938966

Printed on acid-free paper

springer.com

Chapter 24
Measuring Nonlinear Refraction and Its Dispersion

Eric W. Van Stryland and David J. Hagan

Abstract We describe methods for measuring the nonlinear refraction of nominally transparent materials that involve propagation from the near to the far field, which changes a phase distortion into an amplitude redistribution. These methods include beam distortion methods and Z-scan. We also look at methods to determine the spectral dependence of these changes in refractive index. Recent advances here include using femtosecond white-light continua as the source for Z-scan. The types of nonlinear refractive mechanisms are also briefly discussed including bound-electronic, excited state or free-carrier generation, reorientation, electrostrictive, and thermal nonlinear refraction as well as cascaded second-order nonlinearities.

24.1 Introduction

Nonlinear refraction (NLR) is the general name ascribed to phenomena that give rise to an intensity-dependent refractive index. A wide variety of mechanisms can give rise to NLR, and magnitudes and response times can vary by many orders of magnitude for the different mechanisms; however in many cases, the nonlinear refractive index may be adequately characterized by:

$$n(I) = n_0 + \Delta n(I) = n_0 + n_2 I, \tag{24.1}$$

where n_0 is the linear refractive index, I is the irradiance, and n_2 is the nonlinear refractive index. Nonlinear absorption (NLA) and NLR were among the very first nonlinear optical effects reported [1–4]. The experimental study of NLR is typically more complex than for NLA, due to the fact that its effects are usually only observed after some amount of propagation. Essentially, the input beam to a nonlinear material sets up a phase mask whose amplitude profile mimics the

E.W.Van Stryland (✉)
CREOL, The College of Optics and Photonics, University of Central Florida, Orlando, FL 32817, USA
e-mail: ewvs@creol.ucf.edu

R.W. Boyd et al. (eds.), *Self-focusing: Past and Present,*
Topics in Applied Physics 114, DOI 10.1007/978-0-387-34727-1_24,

irradiance profile of the incoming beam. The "lens" thus created with this spatially graded index then either focuses or defocuses the beam upon propagation with the imposed aberrations.

If the sample is thick compared to the focusing length, the nonlinear phase shift may significantly alter the irradiance distribution within the sample. For self-focusing nonlinearities this can have catastrophic consequences (optical damage). If the sample is thin (to be defined later) the alterations in the irradiance distribution occurs only after propagation outside the sample and can be measured, usually in tshe far field. This method of measuring the beam in the far field and comparing to the input beam can determine the sign and magnitude of the nonlinear refraction. Z-scan is a form of this type of measurement. Before describing Z-scan, however, we first look at the beam propagation in Section 24.2. Section 24.3 describes Z-scan and its variants, while Section 24.4 introduces a relatively new technique for measuring the dispersion of nonlinear refraction. This method, referred to as the "white-light continuum Z-scan," relies on high spectral energy density broadband femtosecond continua. Because any discussion of measurement techniques must address the physical processes being measured, in Section 24.5 we briefly discuss several physical mechanisms leading to nonlinear refraction. This leads to questions of how to determine which physical mechanisms are present in any given sample, and ways of unraveling the physics are suggested. An important part of determining the physical mechanisms is determining the dispersion of the nonlinear refraction.

24.2 Beam Propagation

While it is possible to solve the wave equation to calculate the energy distribution at any position along a beam within a nonlinear material, [5–9] for the purpose of quantitatively measuring nonlinear refraction, it is far simpler to use a "thin" sample. By "thin" we mean that the input beam does not change size or shape within the length of the sample, L. This is often referred to as the "external self-action" regime [10]. For this to be valid, neither diffraction nor nonlinear refraction may cause any change of beam profile within the nonlinear sample. The diffraction criterion is simply that the thickness of the sample $L << Z_0$ where Z_0 is the Rayleigh range or depth of focus of the beam. The criterion that NLR does not change the beam shape is $L << Z_0/\Delta\Phi_0$ where $\Delta\Phi_0$ is the maximum nonlinearly-induced phase distortion. This latter requirement simply states that the effective focal length of the induced nonlinear lens in the sample should be much longer than the sample thickness itself [10].

The external self-action limit simplifies the problem considerably, because the amplitude and relative phase, $\Delta\varphi$, of the electric field E inside the nonlinear material are then separately governed by the following pair of simple equations:

$$\frac{d\Delta\phi}{dz'} = \frac{2\pi}{\lambda}\Delta n(I) \tag{24.2}$$

and

$$\frac{dI}{dz'} = -\alpha(I)I, \tag{24.3}$$

where z' is the propagation depth in the sample, I is the irradiance given by $I = n_0 c\varepsilon_0 |E|^2$, with n_0 the linear refractive index, ε_0 the vacuum permittivity, and c the speed of light in a vacuum. The value of $\alpha(I)$ in general includes linear and NLA terms, while Δn includes only nonlinear terms for the index change.

For third-order nonlinearities, where irradiance-induced changes in refraction and absorption are directly proportional to the irradiance, the nonlinear refractive index in the form given in Eq. (24.1) is usually used with the MKS units system. In the Gaussian or cgs units system, n_2 is usually defined as

$$\left\{\frac{n_2}{2}|E|^2\right\}_{esu} = \{n_2 I\}_{MKS}, \tag{24.4}$$

where n_2 is the nonlinear index of refraction, E is the peak electric field (cgs), and I denotes the irradiance (MKS) of the laser beam within the sample. The values of n_2(esu) and n_2(MKS) are related through the conversion formula, $n_2(\text{esu}) = (cn_0/40\pi)n_2(\text{MKS})$. We will use MKS units in this chapter and n_2 will refer to n_2 (MKS). While we are using n_2 here for *any* third-order nonlinearity, it may not be the best description for nonlinearities that have a response slower than the temporal changes in I [11, 12]. The nonlinear absorption may sometimes be written as,

$$\alpha(I) = \alpha_0 + \Delta\alpha = \alpha_0 + \beta I, \tag{24.5}$$

where α_0 is the linear absorption coefficient and β denotes the third-order nonlinear absorption coefficient, which for ultrafast NLA is equal to the two-photon absorption (2PA) coefficient. We qualify this with "sometimes" because often other nonlinear processes cannot be ignored. We will discuss this further in Section 24.5.

When the amplitude and the phase of the beam exiting the sample are known by integrating Eqs. (24.2) and (24.3), the field distribution at the plane of detection can be calculated using diffraction theory (Huygen's principle). The simplest distribution to use, and one that can be experimentally obtained, is a Gaussian beam. Assuming this, and that there is no nonlinear absorption, allows us to calculate the field at a position z' within the thin sample as:

$$E(z', r) = \sqrt{2I_0(z')/nc\varepsilon_0}\, e^{-\left(\frac{r}{w}\right)^2} \exp\left\{ik_0 n_2 I_0(z') e^{-2\left(\frac{r}{w}\right)^2}\right\}, \tag{24.6}$$

where the peak, on-axis input irradiance within the sample is I_0 with a spot size w (half-width at the $1/e^2$ maximum in the irradiance, HW$1/e^2$M). This shows a peak-induced phase distortion at the center of the beam, $\Delta\Phi_0$, of

$$\Delta\Phi_0 = \frac{2\pi}{\lambda} n_2 I_0(L) L_{\text{eff}}, \tag{24.7}$$

with, $L_{\text{eff}} = (l - e^{-aL})/\alpha$. Taking account of the possible temporal structure of the field gives an electric field at the exit of the sample as $E_e(Z,r,t)$, where Z is the position of the sample measured with respect to the input beam waist (in anticipation of Z-scan). In general for radially symmetric systems, a zeroth order Hankel transform of the input electric field will give the field distribution at a distance d from focus.

$$E(Z+d,r,t) = \frac{2\pi}{i\lambda d'} e^{i\frac{\pi r^2}{\lambda z}} \int_0^\infty E\left(Z, r', t - \frac{d'}{c}\right) e^{i\frac{\pi r'^2}{\lambda d'}} J_0\left(\frac{2\pi r r'}{\lambda d'}\right) r' dr', \tag{24.8}$$

where $d' = d - Z$ is the distance from the sample to the position where the field is monitored (again written in this way in anticipation of Z-scan). Here $J_0(x)$ is the zeroth-order Bessel function. There are other ways to calculate the far-field irradiance distribution for Gaussian input beams. See, for example, Ref. [13].

The effects of self-lensing can be easily seen by monitoring the distribution on a camera placed in the far field as shown in Fig. 24.1. Here the sample is placed at or near the beam waist of a Gaussian spatial distribution beam. The peaks are normalized to the same value, and the wings of the beam clearly show the spatial broadening in the far field at high irradiance. This is due to self-focusing in NaCl for which $n_2 > 0$ (known from other data) [14]. For this

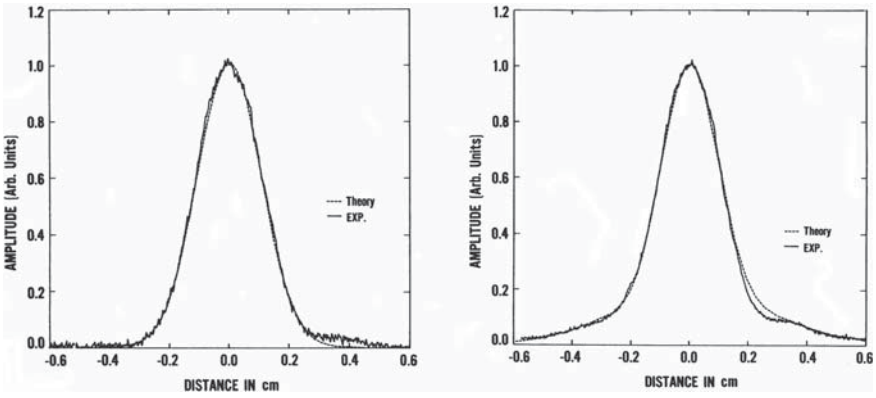

Fig.24.1 Far field fluence distribution after transmission through a 0.5-cm-thick NaCl sample placed at the beam waist of a $\lambda = 532$ nm, ~40 psec FWHM pulse (**a**) at I = 4.7 GW/cm^2 (*left*) and (**b**) I = 57 GW/cm^2 (*right*). Taken from Ref. [14].

geometry, the sign of the nonlinear refraction cannot be deduced from the far-field distribution. In Fig. 24.1(a) the induced-phase distortion is quite large ($\sim$0.5 λ), showing that the sensitivity using this method is not high. The invention of the Z-scan technique provided a simple and sensitive method to determine the sign of the nonlinear refraction which was previously difficult to determine. In order to deduce the sign of the nonlinear refraction the sample can be placed prior to and after the input beam waist. As described in Section 24.3, the beam distortion will then show opposite changes for different signs of Δn. This is key to the success of the Z-scan technique discussed next.

In addition, it is also difficult to separate the contributions of NLA and NLR with only beam distortion measurements. Even two-photon absorption alone leads to beam shape changes with propagation. For example, a Gaussian beam is spatially broadened after propagation through a 2PA material because the center portion of the Gaussian is preferentially absorbed and therefore the diffraction is reduced. This effect is hence similar to self-focusing.

24.3 Z-Scan

Since its invention in 1990, the Z-scan method has quickly gained acceptance as a rapid and sensitive technique for separately determining the nonlinear changes in index and changes in absorption [15–17]. This is primarily due to the simplicity of the technique. In most experiments the index change, Δn, and absorption change, $\Delta\alpha$, can be determined directly from the data without the need for computer fitting. However, the physical mechanisms for Δn and $\Delta\alpha$ cannot be unambiguously determined without other information.

The standard "closed aperture" Z-scan apparatus (i.e., aperture in place in the far field) for determining nonlinear refraction is shown in Fig. 24.2. The input beam is focused and the sample is moved through this focal position in the Z (propagation) direction while the transmittance is monitored in the far field

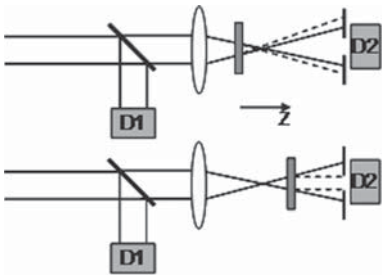

Fig. 24.2 "Closed aperture" Z-scan apparatus. The sample is scanned along "Z," monitoring the transmittance. The solid lines denote the linear focusing while the dotted lines depict the effects of the sample on this propagation assuming a self-focusing nonlinearity. The ratio of the outputs of detectors D2 and D1 is monitored.

through an aperture. The required scan range in an experiment depends on Z_0 and on the sample thickness L. If w_0 is the focal spot size (HW1/e^{2}M), Z_0 is defined as $\pi w_0^2/\lambda$ for a Gaussian beam. For thin samples, the scanning range in Z should be $\sim$ *10* Z_0 although all the information is theoretically contained within a scan range of $\pm Z_0$. This allows the full shape of the Z-scan to be observed and makes interpretation simpler.

A closed aperture Z-scan for a thin sample of BaF_2 exhibiting purely nonlinear refraction at 532 nm, is shown in Fig. 24.3 (left) (solid line). For this material, the change in refractive index, $\Delta n > 0$, resulting in self-focusing which leads to a valley followed by a peak in the normalized transmittance as the sample, is moved away from the lens in Fig. 24.2 (increasing Z). The normalization is performed so that the transmittance is unity for the sample far from focus where the nonlinearity is negligible (i.e., for $|Z| >> Z_0$). The positive lensing in the sample placed before the focus moves the focal position closer to the sample resulting in a greater far-field divergence and a reduced aperture transmittance. On the other hand, with the sample placed after focus, the same positive lensing reduces the far-field divergence allowing for a larger aperture transmittance. The signal for the same magnitude of NLR but with the opposite sign (self-defocusing) is its mirror image, i.e., peak followed by valley (Fig. 24.3, right). Clearly, with the sample at focus the effect of NLR on the transmitted beam is minimized. This explains why the transmitted beam profile shown in Fig. 24.1 shows a very small change despite a quite large nonlinear phase shift.

The change in normalized transmittance for the Z-scan is linear in the induced phase distortion. This is best seen by looking at the change in

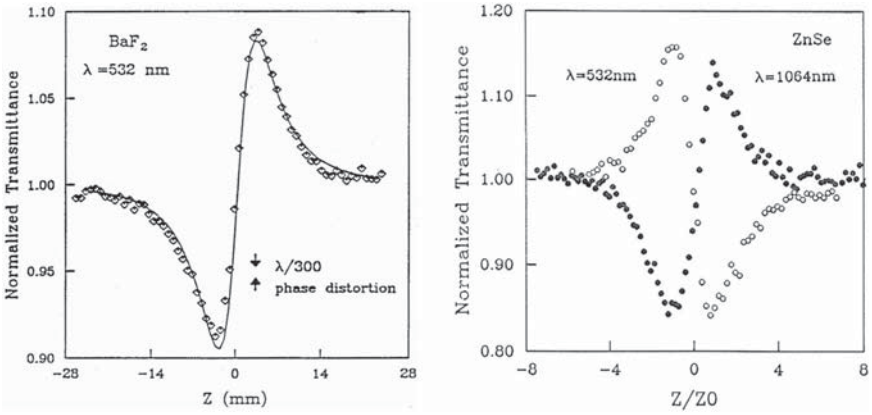

Fig. 24.3 (*left*) Z-scan of BaF_2 at $\lambda = 532$ nm with ~40 ps (FWHM) pulses with the irradiance turned down to show the signal-to-noise ratio allowing phase distortions of $\sim \lambda/300$ to be measured. The overall phase distortion in BaF_2 is $\sim\lambda/14$. Taken from Ref. [16]; (*right*) Closed aperture Z-scan transmittance curves for ZnSe at 1064 nm (*closed circles*) and 532 nm (*open circles*), clearly showing the dispersion of n_2 as it changes from positive at 1064 nm to negative at 532 nm. The second figure is from [18]

transmittance calculated by the difference between the normalized transmittance at the peak, T_p, and valley, T_v, i.e., $\Delta T_{pv} = T_p - T_v$. The relation between the induced phase distortion, $\Delta\Phi_0$, and ΔT_{pv} for a third-order nonlinear refractive process in the absence of NLA is empirically determined to be,

$$\Delta T_{pv} \cong 0.406(1 - S)^{0.27}|\Delta\Phi_0|, \tag{24.9}$$

where S is the transmittance of the aperture in the absence of a sample [16]. This relation is accurate to within ±3% for $\Delta T_{pv} < 1$. As an example, if the induced optical path length change due to the nonlinearity is $\lambda/250$, $\Delta T_{pv} \approx 1\%$ for an aperture transmittance of $S = 0.4$. Figure 24.3 shows an experimental sensitivity of better than $\lambda/300$.

This interferometric sensitivity is one of the most useful features of the Z-scan technique. At first sight this appears rather remarkable given that it is a single-beam method. However, Z-scan is based on propagation to the far field. Propagation results in diffraction, and diffraction is really an interference phenomenon, i.e., interference between different spatial portions of the beam, here the center of the beam interfering with the wings. Thus, Z-scan is effectively a single-beam interferometer and the sensitivity is a result of this interference. In addition, although the optics used are not as good as the sensitivity of the experiment, we must remember that we are looking at the *change* in phase and not the absolute phase.

The size of the aperture in a Z-scan experiment is specified by its transmittance, S, in the linear regime, i.e., when the sample has been placed far away from the focus. The sensitivity to the induced-phase distortion depends on S, going from its highest value for S very small to 0 for $S = 1$ (so-called "open aperture" Z-scan, which is only sensitive to nonlinear absorption, as discussed later). However, values of S from 0.1 to 0.4 work well for only a small loss in sensitivity as seen from Eq. (24.9). This allows a large signal on the detector and averaging over any local spatial beam inhomogeneities.

Equation (24.9) does not include the time averaging that occurs upon detection for short pulse inputs that are normally used in Z-scan experiments. The linear relationship between ΔT_{pv} and $\Delta\Phi_0$ allows us to use a simple multiplication factor, A_τ, which for pulses much shorter than the nonlinear response time, e.g., bound-electronic responses, is given by:

$$A_\tau = \frac{\int_{-\infty}^{+\infty} f^2(t)dt}{\int_{-\infty}^{+\infty} f(t)dt}, \tag{24.10}$$

where $f(t)$ is a function describing the irradiance pulse shape in time. For NLR with an instantaneous response, A_τ depends on the pulse shape. For example, for Gaussian pulses $A_\tau = 1/\sqrt{2}$. However for pulses much shorter than the

response time of the material nonlinearity, $A_\tau = 1/2$ independent of the pulse shape**.** The temporal averaging must be reevaluated in cases involving higher-order nonlinearities.

The accuracy of the measurements of $\Delta\Phi_0$ and thus n_2 depend on how well the laser beam parameters are known, i.e., pulse energy (or power), and temporal and spatial properties [19]. In addition, the Z-scan signal is sensitive to all nonlinear optical mechanisms that give rise to a change of the refractive index (and absorption). Thus, it is not possible from single measurements to determine the origin of the nonlinearity (or nonlinearities). Other information such as the temporal dependence measured in pump-probe experiments is needed for this.

Another quite useful feature of the Z-scan signal is that the distance between peak and valley in Z, ΔZ_{pv} gives a direct measure of the diffraction length of the incident beam. Assuming a third-order nonlinear response using a Gaussian spatial profile beam,

$$\left|\Delta Z_{pv}\right| \approx 1.7 Z_0. \tag{24.11}$$

Given a known thin sample nonlinear response, this is a fast method for determining the spot size and helps to self-calibrate the irradiance for Z-scan.

The previous discussion assumed no nonlinear absorption. Another invaluable feature of Z-scan is its capability to separately and simultaneously measure NLR and NLA. This can be done even when both are present. We do not discuss this in detail here, but by performing two Z-scans, one "closed aperture" (S small) and one "open aperture," $S = 1$, the phase distortion can be extracted. This is easily accomplished in a single experiment using a beam splitter where one of the beams is sent to a detector with an aperture in place and the other beam goes to a detector set to collect all of the transmitted light. The open aperture Z-scan is insensitive to the induced-phase distortion for thin samples, and thus the NLA can be easily determined. The closed aperture Z-scan can then be fit with the known NLA and unknown NLR. However, a quick method to obtain the NLR is to divide the closed aperture Z-scan data (after normalization) by the open aperture Z-scan data (again after normalization). The resulting curve can be used to determine $\Delta\Phi_0$.

The ΔT_{pv} for this curve is essentially the same as the curve for a material with the same NLR but without NLA as long as the ratio of NLA to NLR does not get too large. The criteria for this are given in Ref. [16]. Typical curves for "open" and "closed" aperture Z-scans and their division are shown in Fig. 24.4 where $\Delta\Phi_0 = -0.5$. Other methods such as degenerate four-wave mixing (DFWM) present difficulties in separating the effects of NLR from NLA.

There have been a great number of publications discussing variations of the Z-scan technique. These include: using different beam profiles to increase the sensitivity [21]; eclipsing the Z-scan (EZ-scan) [22], which provides enhanced sensitivity by using a central obscuration disk instead of an aperture; the "2-color Z-scan" that collinearly focuses two beams of different wavelength to

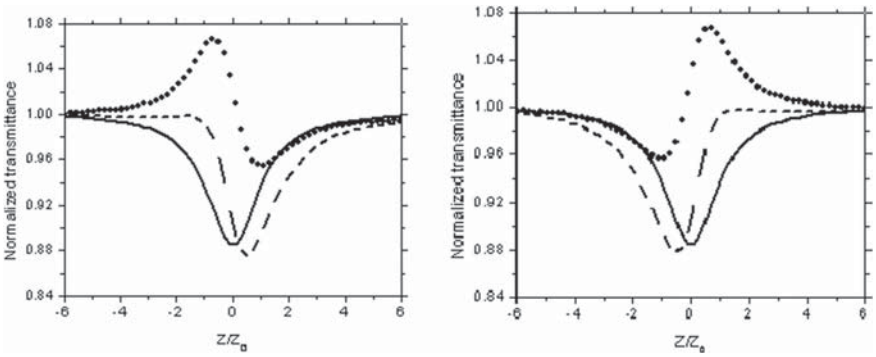

Fig. 24.4 Calculations of closed (*solid line*, $S = 0.5$) and open (*dashed line*) aperture Z-scan data along with their ratio (*dotted line*) for (*left*) self-defocusing and (*right*) self-focusing

measure nondegenerate nonlinearities by Z-scanning [23, 24]; and the time-resolved pump-probe Z-scans, where refractive changes induced by a strong pump pulse are measured [25, 26]; etc. Simple methods have also been developed for analyzing Z-scans where the sample is too thick for the external self-action approximation to hold [27–30].

24.4 Measuring Nonlinear Dispersion

In principle the dispersion of the nonlinear refractive index can be determined by performing Z-scans at many wavelengths, and excellent results have come from such measurements [31]. The same is true of determining nonlinear absorption spectra. Unfortunately, however, this can be difficult and time consuming. It is usually difficult to tune a laser or optical parametric source while keeping the same beam parameters. Hence, careful and time-consuming beam characterization is required at each wavelength to determine the irradiance. The Z-scan helps in determining the spot size (assuming prior knowledge of the order of the nonlinear response), but it gives no information about the temporal dependence. In addition, experience shows that these beam parameters can change from day to day as the laser/parametric source is tuned repeatedly.

Advances in white-light-continuum (WLC) generation [32–34] have resulted in an alternative source for Z-scans in the visible and near IR. Because of the sensitivity of the Z-scan, for many materials only a few nJ of energy are needed when using femtosecond pulses. The spectral energy density of the continuum turns out to be sufficient for measuring materials showing strong nonlinearities [35–37]. However, for materials with low nonlinearities, higher spectral irradiance is sometimes needed. Producing WLC in $\sim$1-m-long cells filled with high-pressure noble gas–filled cells gives much higher spectral irradiance than in solids and

liquids [38, 39]. For example, the WLC spectrum produced by focusing 0.7 mJ of 775 nm, ~140 fs pulses into a 1-m-long chamber filled with Krypton gas at 2.4 atm produces a useful continuum from 400 nm to > 800 nm [39, 40]. This continuum has sufficient spectral energy density over this spectral range for Z-scan. The calculated Rayleigh range within the sample is 8.5 cm [39]. In any ~10 nm spectral band there are many nJ of energy in ~100 fs pulses, which is sufficient for measuring NLR in most materials, e.g., organic dyes in solution [39]. In both methods of continuum generation it is important to maintain good spatial profiles. This requires careful control of the input beam parameters and energy to assure "single filament" operation.

The WLC are often produced by mechanisms that include self-focusing and, in particular, "small-scale" self-focusing can lead to multifilament operation which results in unusable spatial profile beams (see the chapter by Campillo in this book). A single filament operation results in high quality Gaussian-shaped beams. The spatial profile for the continua produced in Kr are Gaussian over the entire 400–800 nm spectral range; however, for longer wavelengths, while there is considerable energy, the spatial profile becomes doughnut-shaped, making Z-scans more difficult to analyze. We briefly describe this WLC Z-scan method below [39].

It is not possible to simply replace the source in the standard Z-scan with the WLC. The problem is that nondegenerate nonlinearities will accompany the degenerate response and, for example, the overall NLR will be considerably increased with no simple way to distinguish the relative contributions of degenerate and nondegenerate NLR. The simplest way around this is to simply spectrally filter the input using narrow band filters, NBF's (or "spike" filters). Other methodologies for spectrally dispersing in space or even in time using group velocity dispersion are possible [36], but are more complicated for measuring NLR given the importance of the spatial profiles in closed aperture Z-scans. The spectral selection can be done by simply introducing NBFs into the beam prior to the sample with care to ensure that they do not disturb the spatial or temporal profile. Automation of such filtering can be done using computer-controlled motorized filter wheels [39].

In addition, there are variable frequency filters available in certain frequency bands (e.g., the entire visible spectrum) where the tuning is continuous (so-called "linear variable filters"). These filters combine spatially varying high pass and low pass filters that are combined to give a spatially varying and wavelength-adjustable NBF. These can be moved laterally changing the transmitted narrow wavelength range continuously. A requirement for any of these NBFs is that the band pass is wide enough to allow short pulse transmittance. For the ~100 fs pulses of many sources, e.g., Ti:sapphire, the ~10 nm bandwidth works well.

With knowledge of the energy, beam size, and pulse duration for each spectral component of the WLC source, standard Z-scans can be performed. The pulsewidths for each spectral region can be determined by various standard techniques [41, 42]. The measured pulsewidths for the aforementioned WLC

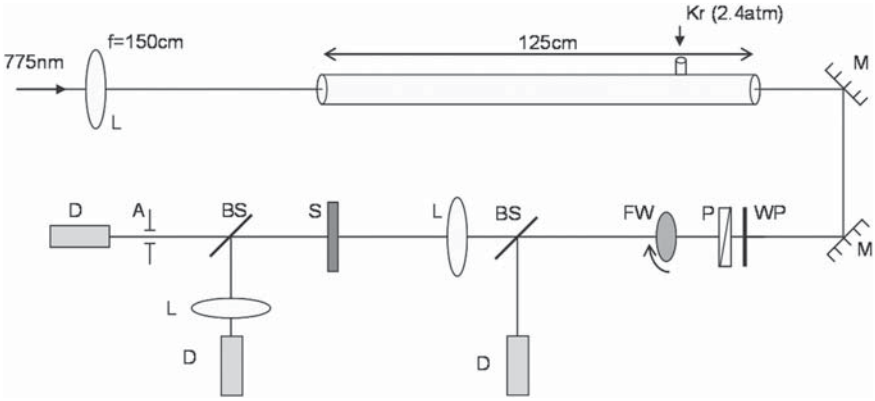

Fig. 24.5 WLC Z-scan experimental set-up: L, lens; M, mirror; WP, half-waveplate; P, polarizer; FW, filter wheel; BS, beamsplitter; D, detector; A, aperture; S, sample. Taken from Ref. [35]

produced in Kr averaged around 90–100 fs and had a time-bandwidth product of ~0.44 for the 10-nm bandpass filters. The advantage of this methodology is that in practice, these WLC are very reproducible from one day to the next so that once characterized, measurements on multiple samples can be rapidly taken over the entire spectral range of the WLC. A typical experimental arrangement is shown in Fig. 24.5.

An example of data taken with this method, displaying data for ZnSe, is shown in Fig. 24.6 (energy gap (E_g) = 2.7 eV with a thickness of 0.5 mm). Here the group velocity dispersion at the shortest wavelengths (<550 nm) is important to take into account as it affects the pulsewidth within the sample (at 480 nm a 28% change is calculated for the pulse between the front and back surfaces, this is the largest effect for ZnSe which linearly absorbs at shorter wavelengths).

The values of β and n_2 corresponding to ZnSe obtained from fits at different wavelengths are presented in Fig. 24.7 along with the theoretical predictions of Refs. [40, 44].

The important point to make concerning these data for n_2 is that the NLR can be measured in the presence of relatively strong NLA and with either positive or negative sign of n_2. In this case, n_2 changes from positive to negative as the ratio of $\hbar\omega/E_g$ goes above $\sim 0.7\ E_g$. This feature of the Z-scan enabled the elucidation of nonlinear Kramers-Kronig relations for ultrafast nonlinearities to connect n_2 to two-photon absorption [45].

24.5 Physical Mechanisms Leading to Nonlinear Refraction

We have discussed two of the primary methods for measuring nonlinear refraction related to propagation of a beam with a near-field phase mask to the far field to redistribute the energy of the beam in space. There are many physical

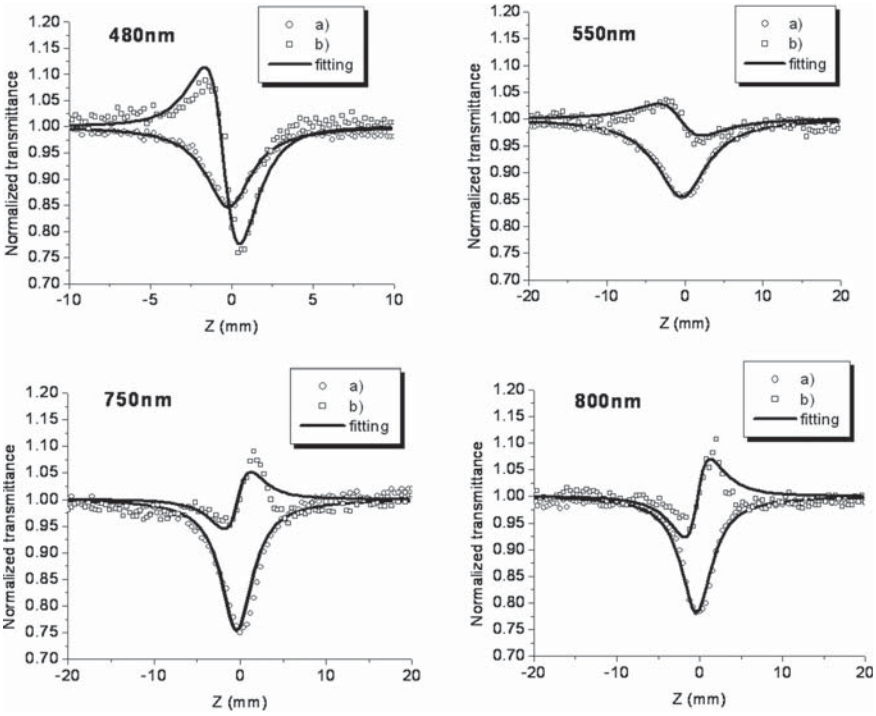

Fig. 24.6 Z-scan data at 480 nm, 550 nm, 750 nm, and 800 nm (**a**) open aperture and (**b**) closed aperture (the result of the division with open aperture). Taken from Ref. [39]

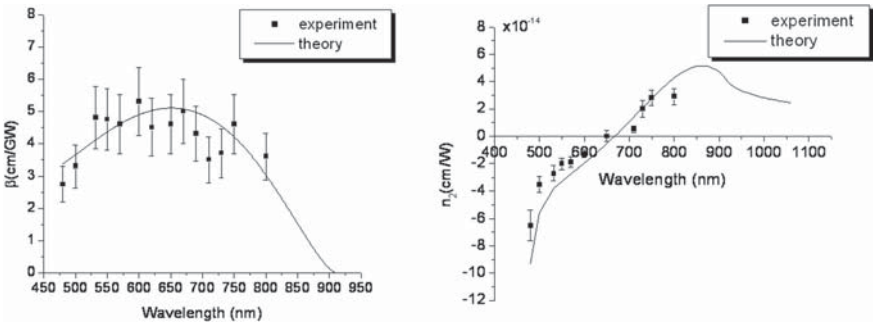

Fig. 24.7 2PA and n2 coefficients of ZnSe obtained from theory and from the experimental data fitting. Taken from Ref. [39]

processes that can lead to the initial phase mask. In this section we briefly discuss a few of these. We begin with the ultrafast, bound-electronic nonlinear refraction from the third-order nonlinear susceptibility, which is accurately

described by the coefficient n_2 in Eq. (24.1). This n_2 is related to the nonlinear absorption of 2PA, etc., through causality and nonlinear Kramers–Kronig relations as described in Refs. [44, 45].

The Z-scan method was essential in allowing NLR to be measured in the presence of NLA in order to see the change in sign of n_2 at photon energies of about 0.7 of the bandgap energies in semiconductors. This sign change of n_2 was a crucial element leading to the full understanding of nonlinear Kramers– Kronig relations [45]. Measurements of these ultrafast responses can now be easily distinguished from slower nonlinearities with the use of femtosecond pulses; however, longer pulses often show other nonlinearities that can mask the faster responses. For semiconductors these include free-carrier nonlinearities from carriers produced via 2PA. Free-carrier refraction becomes substantial for picosecond or longer pulses, and is always negative. (An oscillator is produced with a zero resonance frequency so that one is always above resonance.) For 2PA created carriers, this is an effective fifth-order nonlinearity resulting from the third-order 2PA in combination with the first-order change in the refractive index [18]. In this case, the index change, is given by

$$\Delta n(t) = n_2 I(t) + \sigma_r N(t), \tag{24.12}$$

where σ_r is the free carrier refraction coefficient, and $N(t)$ is the photoexcited carrier density. For 2PA excitation, $N(t)$ is governed by

$$\frac{dN}{dt} = \frac{\beta I^2}{2\hbar\omega} - \frac{N}{\tau}. \tag{24.13}$$

For semiconductors, the lifetime, τ, is typically on the order of nanoseconds, so for picosecond pulses these carriers accumulate with time during the pulse. Because the carrier refraction is quadratic in I, above some input irradiance the carrier refraction will dominate the NLR. For long pulses, the free-carrier effects are almost always dominant unless very low irradiance can be used with a very sensitive technique [18].

In Fig. 24.8, we show streak camera measurements of the transmitted spatial beam profile of a 15 μJ, 30 ps, 532 nm pulse through a 2-mm-thick sample of ZnSe, which exhibits 2PA at this wavelength. We see from the beam profiles, measured every 9.3 ps, that the beam distortion due to nonlinear refraction is much stronger later in the pulse than at early times, as expected where free carrier refraction dominates the bound electronic n_2.

However, extracting values for the n_2 and free carrier refraction coefficient from the data in Fig. 24.8 is not particularly easy. It is preferable to perform a series of Z-scan experiments in order to extract these coefficients. This can be done by taking advantage of the quadratic and linear irradiance dependences of the respective carrier and bound electronic contributions to NLR. First, Z-scans can be taken at low irradiance where the bound electronic n_2 dominates.

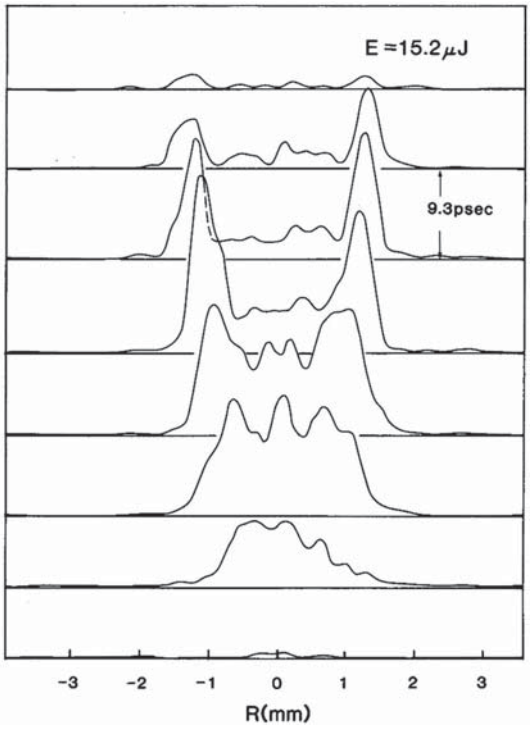

Fig. 24.8 Spatial energy distribution at 11 cm behind a thin (0.2 cm) ZnSe sample at 9.3-ps time intervals as detected by a streak-camera vidicon system for an input energy of 15.2 μJ. Taken from Ref. [46]

As always, we have to perform open and closed aperture Z-scans. In Fig. 24.9, we show open and closed aperture Z-scans on ZnSe with 30-ps pulses at 532 nm. The open aperture Z-scan [Fig. 24.9 (a)] gives us the 2PA coefficient. We find that absorption due to free carriers is negligible in this experiment. This value for the 2PA coefficient is used in fitting a value of n_2 to the closed aperture Z-scan shown in Fig. 24.9(b). [18]

At higher energies, free carrier refraction becomes significant, eventually dominating. The values obtained for β and n_2 at low energies may then be used to fit the final remaining parameter, which is σ_r, the free carrier refraction coefficient. Results of this fitting for higher energies are shown in Fig. 24.10. It should be noted that in these experiments, even at these higher energies, absorption due to the 2PA-excited carriers was insignificant. However, should free-carrier absorption be significant, its value can be found from high-energy open aperture Z-scans, and the rest of the procedure remains the same.

The nonlinearities seen here are also observed in organic dyes; however, the interpretation is nonlinear absorption and refraction from the 2PA generated excited states as opposed to free carriers. Here the sign of the NLR will depend on which side of resonance is the input photon energy [43].

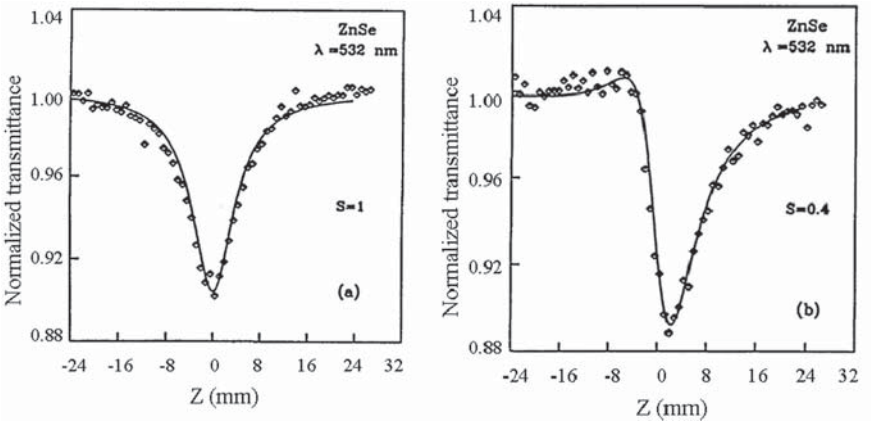

Fig. 24.9 Normalized Z-scan data of a 2.7-mm ZnSe sample measured with 27 ps (FWHM) pulses and $\lambda = 532$ nm at low irradiance ($I_0 = 0.21$ GW/cm^2). The solid curves are the theoretical fits. (**a**) Open-aperture data ($S = 1$) were fitted with $\beta = 5.8$ cm/GW. (**b**) 40%-aperture data were fitted with $\beta = 5.8$ cm/GW and $n_2 = -6.8 \times 10^{-14}$ cm^2/W. Taken from Ref. [18]

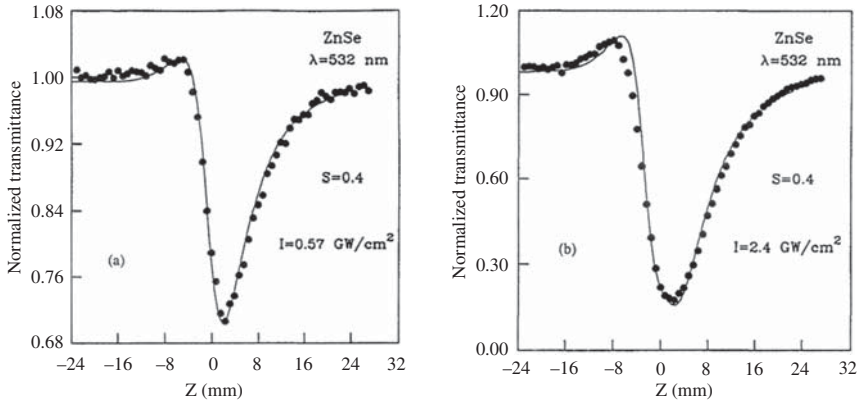

Fig. 24.10 Closed-aperture Z-scan data ($S = 0.4$) and theoretical fits (*solid curves*) of the ZnSe sample taken at high irradiance levels of (*left*) $I_0 = 0.57$ GW/cm^2 and (*right*) $I_0 = .4$ GW/cm^2, where free-carrier refraction is significant. The data were fit with $\beta = 5.8$ cm/GW, $n_2 = -6.2 \times 10^{-14}$ cm^2/W and $\sigma_r = -0.8 \times 10^{-21}$ cm^3. Taken from Ref. [18]

Irradiance dependence studies using beam propagation effects can help in determining the responses along with pulsewidth-dependent studies; however, complementary methods that provide direct information on the temporal response of the nonlinearity such as pump-probe techniques and four-wave mixing are also useful in determining the physical processes involved. [48, 49]

Examples of NLR processes that are easily confused with the bound electronic n_2 because they are effectively third-order, are excited-state refraction from linear absorption–created states (or free carriers), and the refraction associated with saturation. Both are related to population redistribution via causality, i.e., Kramers–Kronig relations [45]. In the case of excited-state refraction, excited states (or free carriers) are produced via linear or 1-photon absorption, and then the refractive index changes due to these excited states (or free carriers) or due to the reduction in the number of ground state absorbers [50]. Here again, the pulsewidths used are important, specifically in relation to the excited-state dynamics. If the pulsewidth is much longer than the decay times, the process will appear just like the ultrafast n_2, while if the pulses are shorter, the material nonlinearity grows within the pulse.

In addition, cascaded second-order nonlinearities [51] appear as third-order responses for low inputs. Here, using second-harmonic generation (SHG) as the example, the loss of two photons at the fundamental frequency to produce the SHG is analogous to 2PA, and the change in phase of the beam for nonphase matched operation is analogous to an index change below or above 2PA resonance (the sign of the effective n_2 from cascading changes from below phase match to above going through zero on phase match) [51].

Some other nonlinear refraction mechanisms including electrostriction and thermal nonlinear refraction are nonlocal requiring propagation in the transverse direction in the beam, again making the temporal response key [52].

The last nonlinearity to mention here is molecular reorientation, also known as the AC Kerr effect. In this nonlinearity, responsible for the $\sim$2 ps nonlinear response of CS_2, the input beam's electric field applies a torque to the molecules which causes a reorientation of the induced dipoles, which then increases the polarizability and thus the index along the direction of the applied field [53]. This nonlinear response of CS_2 is often used as a standard response to compare with; however, this only works for pulses long with respect to their response time.

24.6 Conclusion

Although it has been shown that relative measurements of n_2 can be performed [54] for absolute measurements, in order to give reliable values of the nonlinear refractive index, it is important to note the importance of accurately measuring the laser mode and pulse parameters because n_2 is irradiance dependent. Thus, given the pulse energy, we need to know both the beam area (i.e., spatial beam profile) and the temporal pulsewidth (i.e., temporal shape) in order to determine the irradiance. Any errors in the measurement of irradiance translate to errors in the determination of n_2 as well as any other nonlinear coefficients.

Using beam propagation to allow the induced phase mask from nonlinear refraction to propagate to give a redistribution of irradiance can greatly

facilitate measurements of n_2. Indeed, viewing this propagation or diffraction as an interference between different portions of the beam is what leads to the interferometric sensitivity of the Z-scan. One of the most useful features of this method is its ability to separately measure NLR and NLA, even when both are present. We do not discuss this in detail here (details are given in Ref. [16]) but by performing two Z-scans, one "closed aperture" (S small) and one "open aperture," $S = 1$, the phase distortion can be extracted. Many other methods such as degenerate four-wave mixing (DFWM) have a difficult time in separating the effects of NLR from NLA. Determining the sign of n_2 is key to understanding nonlinear Kramers–Kronig relations.

A series of Z-scans at varying pulsewidths, frequencies, focal geometries, etc., along with a variety of other experiments, are often needed to unambiguously determine the relevant mechanisms. It is always advisable to use several complementary characterization techniques if possible to verify the nonlinear response, and the dispersion of the nonlinear refraction is key to understanding the physical mechanisms. In addition, the spectrum of nonlinear absorption can help determine the dispersion of nonlinear refraction as these quantities are related by causality. Simultaneous knowledge of both will further help in understanding these phenomena.

Acknowledgments We gratefully acknowledge the support of the National Science Foundation over many years, current grant ECS# 0524533. The work presented in this paper represents many years of effort involving colleagues and many former and current students as well as post-doctoral fellows. We thank all those involved and acknowledge their contributions through the various referenced publications. We explicitly thank Mansoor Sheik-Bahae for his many contributions, and Mihaela Balu for help in preparing this manuscript.

References

1. W. Kaiser, C.G.B. Garrett: Two-photon excitation in CaF_2:Eu^{2+}, *Phys. Rev. Lett.*, **7**, 229–231 (1961).
2. G.A. Askaryan: Effects of the gradient of strong electromagnetic beam on electrons and atoms, *Soviet Phys JETP-USSR* **15**(6), 1088–1090 (1962).
3. R.Y. Chiao, E. Garmire, C.H. Townes: Self-trapping of optical beams, *Phys. Rev. Lett.,* **13**, 479–482 (1964).
4. V.I. Talanov: Self-focusing of waves in nonlinear media, *JETP Lett.*, **2**, 138 (1965).
5. Dmitriy I., Kovsh S. Yang et al.: Nonlinear optical beam propagation for optical limiting, *Appl Opt.*, **38**, 5168–5180 (1999).
6. H.P. Nolting, R. Marz: Results of benchmark tests for different numerical BPM algorithms, *IEEE J. Lightware Technol.* **13**, 216–224 (1995).
7. G.P. Agrawal: *Nonlinear Fiber Optics*, Academic Press, New York (1989).
8. M.D. Feit, J.A. Fleck, Jr.: Simple method for solving propagation problems in cylindrical geometry with fast Fourier transforms, *Opt. Lett.*, **14**, 662–664 (1989).
9. S. Hughes, J.M. Burzer, G. Spruce et al.: Fast Fourier transform techniques for efficient simulation of Z-scan measurements, *J. Opt. Soc. Am. B*, **12**, 1888–1893 (1995).
10. A.E. Kaplan: External self-focusing of light by a nonlinear layer, *Radiophys. Quant. Electron.*, **12**, 692–696 (1969).

11. R.W. Boyd: *Nonlinear Optics*, Academic Press, San Diego (2003).
12. R.W. Hellwarth: Third-order optical susceptibilities of liquids and solids, *Progr. Quant. Electron.*, **I.5**, 1–68 (1979)
13. D. Weaire,. B.S. Wherrett, D.A.B. Miller et al.: Effect of low-power nonlinear refraction on laser-beam propagation in InSb, *Opt. Lett.*, **4**, 331–333 (1979).
14. W.E. Williams, M.J. Soileau, E.W. Van Stryland: Optical switching and n_2 measurements in CS_2, *Opt. Commun.*, **50**, 256 (1984).
15. M. Sheik-bahae, A.A. Said, E.W. Van Stryland: High-sensitivity, single-beam n_2 measurements, *Opt. Lett.*, **14**, 955–957 (1989).
16. M. Sheik-Bahae, A.A. Said, T.H. Wei, D.J. Hagan, E.W. Van Stryland: Sensitive measurement of optical nonlinearities using a single beam, *IEEE J. Quant. Electron.,* **26**, 760 (1990).
17. P.B. Chapple, J. Staromlynska, J.A. Hermann et al.: Single-beam Z-scan: measurement technique and analysis, *J. Nonl. Opt. Phys. Mat.*, **6**, 251 (1997).
18. A.A. Said, M. Sheik-Bahae, D.J. Hagan et al.: Determination of bound and free-carrier nonlinearities in ZnSe, GaAs, CdTe, and ZnTe, *J. Opt. Soc. Am. B*, **9**, 405–414 (1992).
19. S. Hughes, J.M. Burzler: Theory of Z-scan measurements using Gaussian–Bessel beams, *Phys. Rev. A* **56**, R1103 (1997).
20. E.W. Van Stryland, M. Sheik-Bahae: Z-scan. In: *Characterization Techniques and Tabulations for Organic Nonlinear Optical Materials*, pp. 655–692, M. Kuzyk, C. Dirk (eds.), Marcel Decker, New York (1998).
21. W. Zhao, P. Palffy-Muhoray: Z-scan measurements of χ^3 using Top-Hat beams, *Appl. Phys. Lett.,* **65**, 673–675 (1994). See also, W. Zhao, J.H. Kim, P. Palffy-Muhoray: Z-scan measurements on liquid crystals using Top-Hat beams, *Appl. Phys. Lett.*, **65**, 673–675 (1994).
22. T. Xia, D.J. Hagan, M. Sheik-Bahae et al.: Eclipsing Z-scan measurement of $\lambda/10^4$ wavefront distortion, *Opt. Lett.*, **19**, 317–319 (1994).
23. H. Ma, A.S. Gomez, Cid B. de Araujo: Measurement of nondegenerate optical nonlinearity using a two-color single beam method, *Appl. Phys. Lett.*, **59**, 2666 (1991).
24. M. Sheik-Bahae, J. Wang, J.R. DeSalvo et al.: Measurement of nondegenerate nonlinearities using a 2-color Z-scan, *Opt. Lett.*, **17**, 258–260 (1992).
25. J. Wang, M. Sheik-Bahae, A.A. Said et al.: Time-resolved Z-scan measurements of optical nonlinearities, *J. Opt. Soc. Am. B*, **11**, 1009–1017 (1994).
26. V.P. Kozich, A. Marcano, F. Hernandez et al.: Dual-beam time-resolved Z-scan in liquids to study heating due to linear and nonlinear light absorption, *Appl Spectrosc*, **48**, 1506–1512 (1994). See also J. Castillo, V. Kozich, A. Marcano: Thermal lensing resulting from one- and two-photon absorption studied with a two-color time-resolved Z-scan, *Opt. Lett.*, **19**, 171–173 (1994).
27. M. Sheik-Bahae, A.A. Said, D.J. Hagan et al.: Nonlinear refraction and optical limiting in "thick" media, *Opt. Eng.*, **30**, 1228–1235 (1990).
28. J.A. Hermann, R.G. McDuff: Analysis of spatial scanning with thick optically nonlinear media, *J. Opt. Soc. Am. B*, **10**, 2056–2064 (1993).
29. J.-G. Tian, W.-P. Zang, C.-Z. Zhang et al.: Analysis of beam propagation in thick nonlinear media, *Appl. Opt.*, **34**, 4331–4336 (1995).
30. P.B. Chapple, J. Staromlynska, R.G. McDuff: Z-scan studies in the thin- and the thick-sample limits, *J. Opt. Soc. Am B*, **11**, 975–982 (1994).
31. B. Lawrence, W. Torruellas, M. Cha et al.: Identification and role of two-photon excited states in a π-conjugated polymer, *Phys. Rev. Lett.*, **73**, 597–600 (1994).
32. R.R. Alfano, S.L. Shapiro: Emission in the region 4000 and 7000 • via four-photon coupling in glass, *Phys. Rev. Lett.*, **24**, 584–587 (1970).
33. P.B. Corkum, C. Rolland: Supercontinuum generation in gases, *Phys. Rev. Lett.*, **57**, 2268–2271 (1986).

34. A. Brodeur, S.L. Chin: Ultrafast white-light continuum generation and self-focusing in transparent condensed media, *J. Opt. Soc. Am. B*, **16**, 637–650 (1999).
35. G.S. He, T.C. Lin, P.N. Prasad et al.: New technique for degenerate two-photon absorption spectral measurements using femtosecond continuum generation, *Opt. Express*, **10**, 566 (2002).
36. M. Balu, J. Hales, D.J. Hagan et al.: White-light continuum Z-scan technique for nonlinear material characterization, *Opt. Express*, **12**, 3820 (2004); see also, M. Balu, J. Hales, D.J. Hagan et al.: Dispersion of nonlinear refraction and two-photon absorption using a white-light continuum Z-scan, *Opt. Express*, **13**, 3594 (2005).
37. L. De Boni, A.A. Andrade, L. Misoguti et al.: Z-scan measurements using femtosecond continuum generation, *Opt. Express*, **12**, 3921 (2004).
38. H.R. Lange, G. Grillon, J.-F. Ripoche et al.: Anomalous long-range propagation of femtosecond laser pulses through air: moving focus or pulse self-guiding? *Opt. Lett.*, **23**, 120–122 (1998).
39. M. Balu, D.J. Hagan, E.W. Van Stryland: High spectral irradiance white-light continuum Z-scan, *Proceedings Ultrafast Phenomena Conference*, Monterey, CA, Springer-Verlag, New York (2006).
40. M. Kolesik, E.M. Wright, A. Becker et al.: Simulation of third-harmonic and supercontinuum generation for femtosecond pulses in air, *Appl. Phys. B*, **85**, 531–538 (2006).
41. R. Trebino, Frequency-Resolved Optical Gating: The Measurement of Ultrashort Laser Pulses, Kluwer Academic Publishers, New York (2000).
42. W. Rudolph, M. Sheik-Bahae, A. Bernstein, L.F. Lester: Femtosecond autocorrelation measurements based on two-photon photoconductivity in ZnSe, *Opt. Lett.*, **22**, 313–315 (1997).
43. E.W. Van Stryland, M.A. Woodall, H. Vanherzeele et al.: Energy band-gap dependence of two-photon absorption, *Opt. Lett.*, **10**, 490 (1985).
44. M.Sheik-Bahae, D.C. Hutchings, D.J. Hagan et al.: Dispersion of bound electronic nonlinear refraction in solids, *IEEE J. Quant. Electron.*, **27**, 1296 (1991).
45. D.C. Hutchings, M. Sheik-Bahae, D.J. Hagan et al.: Kramers–Kronig relations in nonlinear optics, *Opt. Quant. Electron.*, **24**, 1–30 (1992).
46. E.W. Van Stryland, Y.Y. Wu, D.J. Hagan et al.: Optical limiting with semiconductors, *J. Opt. Soc. Am. B,* **5**, 1980–1989, (1988).
47. A.A. Said, C. Wamsley, D.J. Hagan et al.: Third- and fifth-order optical nonlinearities in organic materials, *Chem. Phys. Lett.*, **228**, 646–650 (1994).
48. R.S. Lepkowicz, O.V. Przhonska, J.M. Hales et al.: Excited-state absorption dynamics in polymethine dyes detected by polarization-resolved pump-probe measurements, *Chem. Phys.,* **286**(2–3), 277–291 (2003).
49. E.J. Canto-Said, D.J. Hagan, J. Young et al.: Degenerate four-wave mixing measurements of high-order nonlinearities in semiconductors, *IEEE J. Quant. Electron.,* **27**, 2274–2280 (1991).
50. T.H. Wei, D.J. Hagan, M.J. Sence et al.: Direct measurements of nonlinear absorption and refraction in solutions of phthalocyanines, *Appl. Phys. B*, **54**, 46–51 (1992).
51. R. DeSalvo, D.J. Hagan, M. Sheik-Bahae et al.: Self-focusing and self-defocusing by cascaded second-order effects in KTP, *Opt. Lett.*, **17**, 28–30 (1992).
52. D.I. Kovsh, D.J. Hagan, E.W. Van Stryland: Numerical modeling of thermal refraction in liquids in the transient regime, *Opt. Express*, **4**, 315 (1999).
53. D. McMorrow, W.T. Lotshaw, G. Kenney-Wallace: Femtosecond optical Kerr studies on the origin of the nonlinear responses in simple liquids, *IEEE J. Quant. Electron.*, **24**, 443–454, (1988).
54. R.E. Bridges, G.L. Fischer, R.W. Boyd: Z-scan measurement technique for non-Gaussian beams and arbitrary sample thickness, *Opt. Lett.*, **20**, 1821 (1995).